Korean J. Chem. Eng., 39(4), 1072-1077 (2022)
DOI: 10.1007/s11814-021-0974-2

pISSN: 0256-1115
eISSN: 1975-7220

Sound absorption improvement of polyurethane foam through sequential arrangement of its cellular morphology

Hyeon Jun Choi and Jung Hyeun Kim†

Department of Chemical Engineering, University of Seoul, 163 Seoulsiripdae-ro, Dongdaemun-gu, Seoul 02504, Korea
(*Received 26 August 2021 • Revised 1 October 2021 • Accepted 5 October 2021*)

Abstract−We designed four distinct polyurethane foam (PUF) cellular morphologies by employing low-molecular-weight polyols and two types of gelling catalysts. The cellular morphologies contained cavity sizes ranging from 458 μm to 287 μm and open porosities between 0.97 and 0.63. The highest values of the sound absorption coefficient from the four individual specimens were observed at specific frequencies (1,550, 2,000, 2,650, 3,800 Hz) owing to their distinct morphological characteristics. Specimen combinations showed enhanced sound absorption compared to their individual specimens due to the synergistic effect between its highly open porosity, which dissipates high-frequency waves, and its small cavity, which diffracts low-frequency waves. The acoustic activity reached to the highest (0.82) value from the double-layered sample with the front small and back large cavities. The small front cavities resulted in a high noise reduction coefficient because of the destructive interference effect of the low-frequency waves through the relatively large cavity of the back layer. However, its reversely arranged specimen showed increased noise reduction coefficient (0.53) due to the air gap effect. Therefore, suitable layer combinations of the different cellular structures can assist in achieving high sound absorption in PUF systems and be utilized in various practical engineering applications.

Keywords: Polyurethane, Sound Absorption, Layered Foam, Morphology, Noise Reduction Coefficient

INTRODUCTION

Polyurethane foam (PUF) is commonly used in a variety of industrial applications, including cushioning, sound absorption, and thermal insulation, owing to its low density and ease of production [1-6]. In particular, to reduce living and industrial noise, flexible PUF has attracted significant attention as a sound absorption material because of its lightweight nature (porosity>90%). Two types of damping mechanisms, viscous damping with gas molecules and structural damping by cell morphology, play a crucial role in achieving ultimate sound absorption material performance [7-9]. Among the two damping mechanisms, a structural damping mechanism is more important in achieving high sound absorption through flexible PUFs because a viscous molecular damping mechanism is unlikely to change in different air conditions. In general, cavities and pores can serve as active sites to dissipate sound waves by collision of the sound waves with the cell walls and by altering the wave passages via partially open pores. Thus, it is extremely important to understand the structure-property relationship between the cellular morphology and sound absorption coefficient of the PUFs.

There are several reports on the effects of cavity and pore structures on the sound absorption behavior of flexible PUF systems with incorporation of base formulations, additional fillers [10-13], and processing parameters [14-16]. For example, Kim et al. reported the effects of experimental components, such as catalysts and cross-linking agents, on the cellular morphology of PUFs [17]. In their study, the diethanolamine crosslinker strongly influenced the formation of the pore morphology by preventing phase separation in the PU matrix; thus, the best sound absorption was achieved when using the optimum amount of crosslinker. Choe et al. determined that the type of isocyanate structure (aromatic and aliphatic) used in the fabrication of flexible PUFs is strongly related to its pore structure owing to the difference in electrophilicity and steric hindrance between the aromatic and aliphatic isocyanate groups [18]. Thus, the optimum acoustic activity depends on the aliphatic isocyanate content. Regarding additional fillers, Wang et al. reported the influence of rice hulls on the formation of pore structures in PUFs and the acoustic performances of these PUFs [19]. As the rice hull content increased, the sound absorption peak shifted towards a lower frequency range due to changes in the pore morphology. Chen et al. used biodegradable natural bamboo leaf particles to manufacture PUFs, and examined their acoustic properties [20]. The results illustrated that suitable constituent of the bamboo chips and stems significantly enhanced the sound absorption properties of the PU composite foams over the entire frequency range, specifically, with a considerable improvement in the low frequency range. Oh et al. investigated PUF sound absorbers containing graphene oxide particles which were incorporated by directional alignment in a two-step manufacturing process [21]. The porous graphene sound absorber exhibited a hierarchical cellular structure with adjustable stiffness and an improved sound absorption performance. Sung et al. also reported the relationship between cell morphology and directional sampling locations of PUFs formed by a free-rising process [22]. The small spherical cavities obtained in the horizontal planes resulted in a higher sound absorption coefficient than

†To whom correspondence should be addressed.
E-mail: jhkimad@uos.ac.kr

the irregular elliptical cavities formed in the vertical planes, owing to the higher cavity distribution homogeneity in the horizontal planes.

In most of the abovementioned flexible PUF studies, the sound absorption behavior was investigated at frequencies higher than approximately 2,000 Hz. However, high sound absorption performance in the low-frequency range (lower than 2,000 Hz) was mostly not achieved with these PUFs because of the limitations associated with control over the reaction parameters during the in-situ gelling and blowing processes. For example, homogeneous small cavities with well-distributed pores on the cavity walls are generally advantageous for high sound absorption in the low-frequency range [7,8]. Therefore, several examples of porous metal foams, which form robust small cavities and pores, have recently been reported, as they exhibit high sound absorption efficiency in the low-frequency range [23-25]. Because of the superior benefits of flexible PUFs in commercial applications, in this study we further explored their sound absorption performance. Therefore, we devised a multi-layered PUF structure to improve the sound absorption performance from low- to high-frequency ranges by incorporating distinct PUF morphologies in the separate layers. To manipulate the morphology of the foam, the molecular weight of the polyol and types of gelling catalysts used were chosen as control parameters to synthesize PUFs with different morphologies. Four different types of foam morphologies were used in the different combinations of double-layered PUF structures. The effect of the sequence arrangement of the foam morphologies on the ultimate acoustical performances was systematically investigated.

METHODS

1. Materials

Polyether polyols PPG-6000 (Kumho Petrochemical, Korea, OH value: 28±2, M_w: 6,000 g/mol, f_{av} (the average functionality)=3, μ= 1,200±100 cps at 25 °C), TF-400 (Mitsui Chemicals & SKC Polyurethanes Inc., Korea, OH value: 400±15, M_w: 400 g/mol, f_{av}=3, μ=350±50 cps at 25 °C), and aromatic diisocyanate COSMONATE CG-3701S (Kumho Mitsui Chemical, Korea, %NCO: 37±0.5, μ= 15 cps at 25 °C) were used in the synthesis of the polyurethane foams. To catalyze the gelling and blowing reactions, DABCO 33LV (Air Products and Chemicals, USA, 33% triethylenediamine and 67% dipropylene glycol), DABCO BL11 (Air Products and Chemicals, USA, 70% bis(2-dimethylaminoethyl) ether diluted with 30% dipropylene glycol), and dibutyltin dilaurate (DBTDL, Sigma-Aldrich, USA) were used. Silicon surfactant L-3002 (Momentive, USA, ν=42 cps at 25 °C) was used to achieve homogeneous cellular distributions and diethanolamine (DEA, Sigma-Aldrich, USA, M_w: 105 g/mol) was used as a crosslinking agent. Deionized water was used as a blowing agent to generate the cellular foam structures.

2. Synthesis

First, the polyol systems were prepared by mixing the polyol, catalyst, crosslinker, blowing agent, and surfactant at 1,700 rpm for 10 min in 1 L paper cups. Subsequently, equivalent amounts of isocyanate, to achieve an NCO index of 1.0, were added to the pre-mixed polyol systems and further mixed at 6,000 rpm for 7 s to form homogeneous mixtures. Next, the PU mixtures were quickly poured into an aluminum mold (200 mm×200 mm×50 mm) and cured at 60 °C for 20 min. Finally, the foams were removed from the mold and stored at room temperature under a relative humidity of 50% for three days before cutting the specimens. All the specimens were prepared using the PU sample core, except for the foam skin (10 mm). In general, the urethane linkages are formed through reactions between the hydroxyl and isocyanate groups, and the cellular foam structure is simultaneously produced from CO_2 gas generated from the reaction between the water molecules and the isocyanate groups. During CO_2 gas generation, the cell morphology develops through these sequential steps: cell nucleation, cavity growth, and pore generation through contact with the adjacent cavities [26]. In addition, the types (open, partially open, closed) of pore structure strongly depended on the reaction kinetics of the PUF and the physical strength of the cell walls [27].

Table 1. Formulation details of the flexible PUFs exhibiting variable morphologies

Components		Formulation (g)			
		A	B	C	D
Poloyol1	PPG6000	100	100	25	25
	molar ratio	1.0	1.0	0.25	0.25
Polyol2	TF400	-	-	5.19	5.19
	molar ratio			0.75	0.75
Catalyst1	DABCO33LV	0.72			
Catalyst2	DABCOBL11	0.08			
Catalyst3	DBTDL	-	0.10	-	0.10
Crosslinker	DEA	4.00			
Blowing agent	Water	0.60			
Surfactant	L-3002	1.32			
Isocyanate	CG-3701S	57.3*			

*NCO index: 1.0.

To manufacture the PUFs, a polyol system, which included a polyol, catalyst, crosslinker, blowing agent, and surfactant, was first weighed and mixed, followed by the addition of isocyanate to the pre-mixed polyol system to complete the PU reaction. Details regarding the amounts of the components used are summarized in Table 1. Four different formulations, in which the polyol molecular weight and the type of gelling catalyst were varied, were selected to include a wide range of cavity and pore sizes. Sample A, exhibiting the largest cavity and pore sizes, was considered the reference foam. Then, the cavity and pore sizes were reduced by combining a metallic gelling catalyst and low-molecular-weight polyol with the reference formulation to produce samples B and C. Finally, the smallest cavity and pore sizes were formed by combining two parameters in sample D.

3. Morphology

Scanning electron microscopy (SEM, SNE3000M, SEC, Korea, at 15 kV) was used to examine the distinct cellular morphology of samples A, B, C, and D. The PUF specimens were cut and sputter-coated with gold before conducting the analysis. After acquiring the SEM images, Image-Pro Plus software (Media Cybernetics) was used to analyze the cell morphology (cavity and pore sizes), using

20 images to minimize statistical uncertainty. In addition, the cell wall area ratio and open porosity were calculated using the following equations:

$$\text{Open porosity}=(N_o+N_p/2)/(N_o+N_p+N_c), \quad (1)$$

$$\text{Cell wall area ratio}=1-(\text{pore area/cavity area}), \quad (2)$$

where N_o, N_p, and N_c are the numbers of open, partially open, and closed pores, respectively [12,28].

3. Sound Absorption Measurements

To determine the sound absorption coefficients of the materials, two impedance tubes (SW420 and SW470, BSWA) containing two 1/4-in microphones (MPA416, BSWA) were used. Two microphones were used to include both the low-mid (63-1,600 Hz) and high (1,000-6,300 Hz) frequency ranges. The sound absorption coefficients for the low-, mid-, and high-frequencies ranges were combined using VA-Lab software (BSWA) to produce single-range plots. The cylindrical PUF samples were 20 mm thick and 100 mm and 30 mm in diameter for the low-and high-frequency ranges, respectively. The sound absorption coefficients were measured according to ISO 10534-1 based on the standing wave ratio.

RESULTS AND DISCUSSION

Scanning electron microscopy (SEM) and Image-Pro Plus software were used to characterize the cellular morphology of the PUF

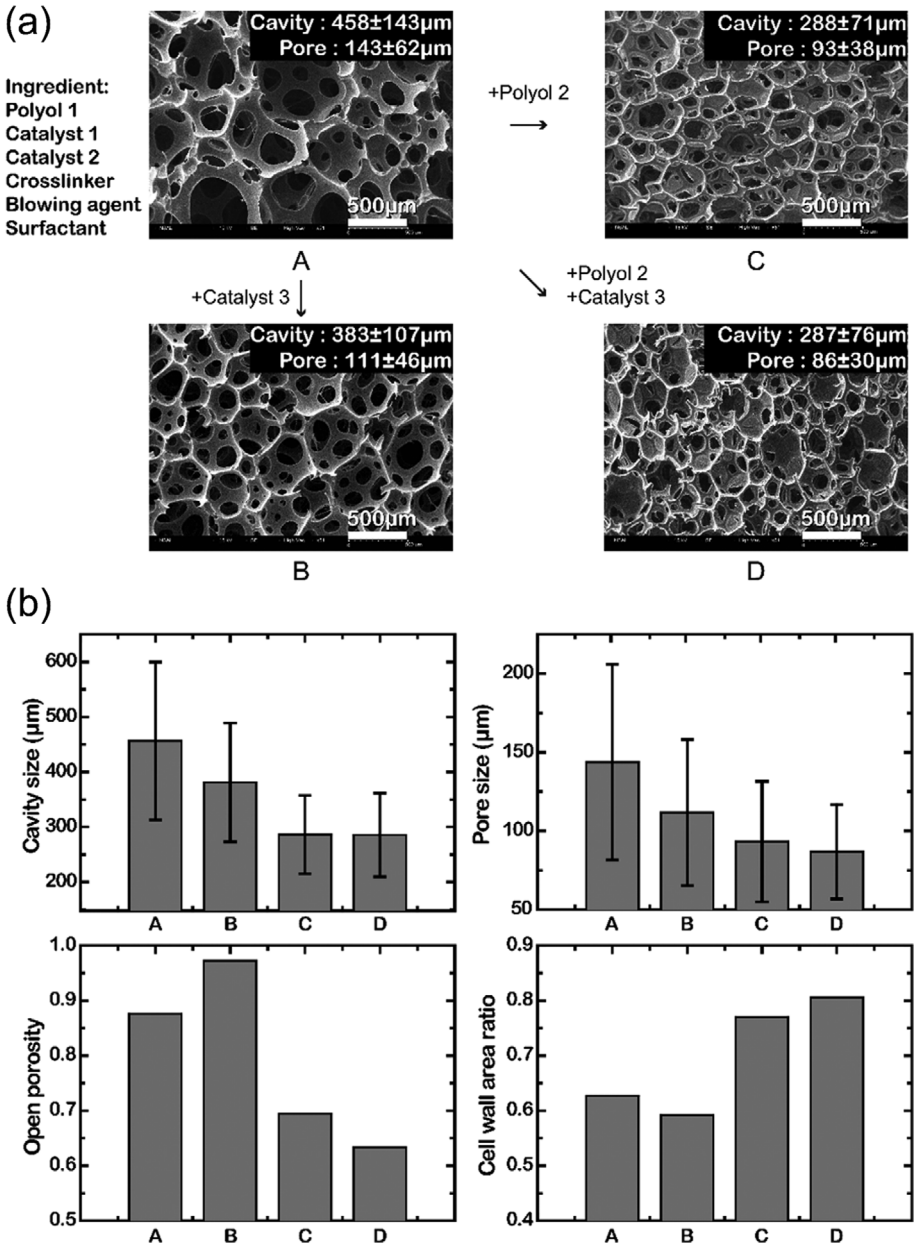

Fig. 1. (a) SEM images of the four PUF samples (detailed formulations for A, B, C, and D are included in Table 1); (b) their cavity and pore sizes with standard deviations, open porosity, and cell wall area ratio.

samples. Fig. 1(a) shows the SEM images of the four samples (A, B, C, and D), including their average cavity and pore sizes with standard deviation. By introducing a small amount (10%) of metallic gelling catalyst (dibutyltin dilaurate, DBTDL), the overall gelling reaction can be accelerated through the synergistic effect of DBTDL and the 1,4-diazabicyclo [2,2,2] octane catalyst (DABCO 33LV) during the PU formation reaction. For example, the higher gelling reaction rate of DBTDL (144 L^2g^{-1} $mol^{-1}h^{-1}$) compared to DABCO 33LV (109 L^2g^{-1} mol^{-1}h, used as the reference sample) produced a higher PU matrix strength during cell growth. The higher matrix strength can result in a smaller cavity size owing to reduced cellular growth during the cavity expansion period. In addition, by combining the low-molecular-weight polyol (TF400, M_w: 400 $gmol^{-1}$) with the base polyol (M_w: 6,000 $gmol^{-1}$), the PU matrix becomes more rigid because of the additional smaller flexible units; therefore, cavity growth is retarded. These two experimental parameters effectively inhibited the overall cellular growth rate during the gelling and blowing reactions. Consequently, the cavity and pore sizes of sample D decreased from 458 (±143) μm and 143 (±62) μm to 287 (±76) μm and 86 (±30) μm, respectively, compared with reference sample A. Fig. 1(b) summarizes the cellular morphology (cavity and pore), including the open porosity and cell wall area ratio of the PUFs. With the addition of DBTDL and TF400 (sample D), the cell wall area ratio increases, but the open porosity decreases because the pore growth is diminished by the high matrix strength. These factors play a significant role in determining the sound wave passages through the cavities and pores in the PUFs. As reported in literature [11,12], the open porosity can be calculated using the numbers of open, partially open, and closed pores; this is extremely useful for analyzing the sound absorption properties of the materials. In addition, the cell wall area ratio was assessed, taking into account the actual cavity surface area excluding pore portions. Choi et al. [28] reported an applicable example of the morphological relationship between the cell wall area ratio and the sound absorption properties of PUFs.

Four samples were used to analyze the sound absorption performance of the PUFs using an impedance tube method. Fig. 2 shows the sound absorption coefficient, acoustic activity (AA), and noise reduction coefficient (NRC) results of the monolayer specimens. The AA (averaging the sound absorption coefficients over the entire frequency range between 63 and 6,300 Hz) [12,29] and NRCs (averaging the sound absorption coefficients at 250, 500, 1,000, and 2,000 Hz) [2,30] were also extracted from the sound absorption coefficient results. These two typical representative sound absorption values can also be expressed by the following equations:

$$AA = \int_{63}^{6300} \alpha \ d(Hz), \quad (3)$$

$$NRC = \Sigma_{i=250,\ 500,\ 1{,}000,\ 2{,}000\ Hz} \alpha_i / 4, \quad (4)$$

where α and α_i are the sound absorption coefficients at specific frequencies. The AA estimates the overall sound absorption performance, while the NRC evaluates the interior noise performance. In Fig. 2(a), the peak location of the sound absorption coefficient is shifted from a high to a low frequency with a sequential decrease in the cavity and pore sizes (shown in Fig. 1). Generally, porous

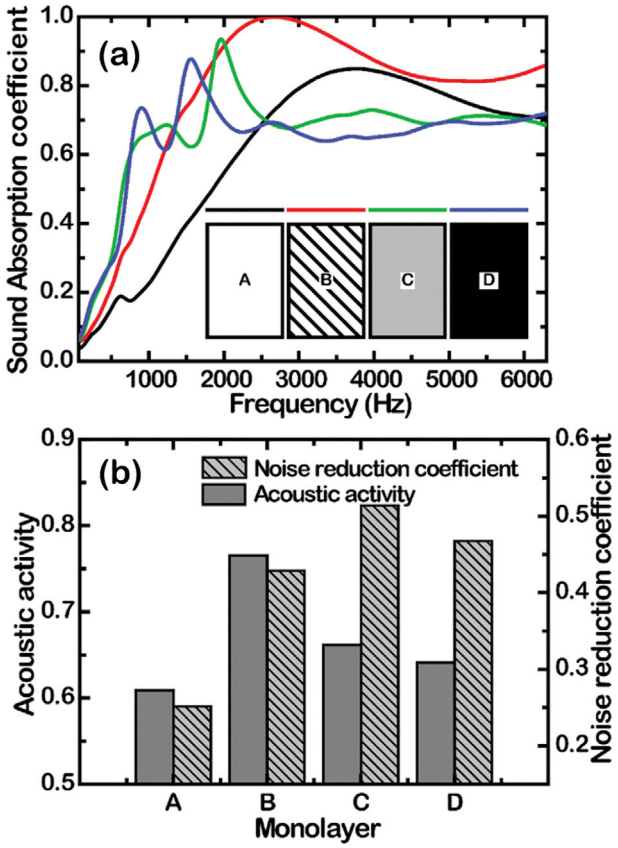

Fig. 2. (a) Sound absorption coefficients and (b) acoustic activity and noise reduction coefficients of the four PUFs.

materials with smaller cavity and pore sizes exhibit higher airflow resistivity and tortuosity because of increased hindrances for air molecule passage. An increase in the tortuosity results in a shift in the sound absorption coefficient peak location to a lower frequency range by matching the total tortuosity length with a quarter wavelength of the sound waves [7]. Additionally, a clear second peak is observed in the sound absorption curve at integer multiples of the wavelength. The curve of sample D shows an increased sound absorption coefficient with a sharp second peak in the low-frequency range. Fig. 2(b) shows that the highest AA is achieved with sample B, while the highest NRC is achieved with sample C. These results are attributed to the method of data extraction and the different cavity and pore sizes between the samples. Based on the acoustic behavior from the four distinct cellular morphologies, the double-layered foam systems were further investigated to improve the sound absorption coefficients of the PUFs over wide frequency ranges.

The combination of different cellular morphologies in the double-layered structures is advantageous for achieving high sound absorption by the PUFs over a wide frequency range. For example, as shown in Fig. 3(a), low-frequency waves generally pass through the cavities and pores in the foams through a diffraction mechanism. Thus, the more obstacles (cell walls per unit volume) the waves encounter, the more efficient the sound absorption. In contrast, for the high-frequency waves, reflection from the cavity walls is the dominant sound absorption mechanism; thus, the reflected

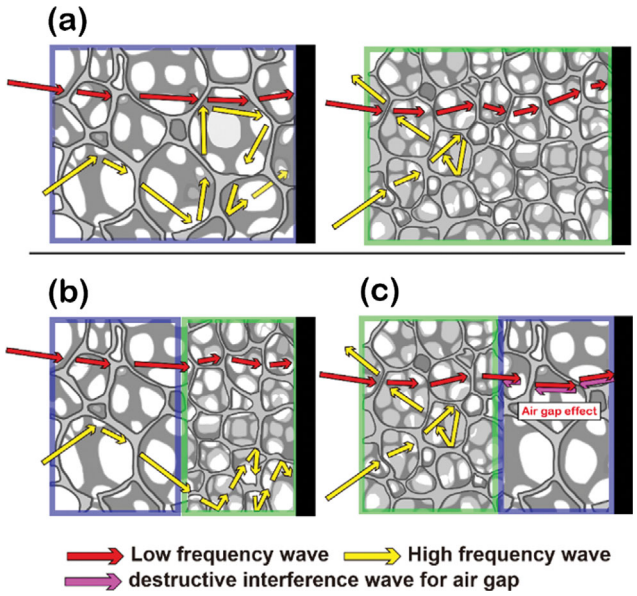

Fig. 3. Illustrations of the sound absorption mechanisms of the low and high frequency waves through the cellular structures. (a) Schematic wave transfer mechanisms in the relatively large and small cavities and pores. The low and high frequency wave sound absorptions are generally achieved through diffraction and reflection mechanisms, respectively. Propagation of the sound waves in the double-layered specimens containing combinations of (b) large cavities in the front and (c) small cavities in the front.

waves can be passed into deeper cavities through the open pores. Therefore, it is necessary to find the best combination of multilayered samples containing various cellular morphologies to achieve high sound absorption throughout the entire frequency range. Fig. 3 shows illustrations of the sound absorption mechanisms applicable for the high- and low-frequency waves. The two typical combinations of cellular morphology revealed a clear difference in sound absorption. Fig. 3(b) indicates the synergistic combination of morphologies for high sound absorption for both the low- and high-frequency waves. In addition, Fig. 3(c) shows the reverse combination to the sample in Fig. 3(b). Furthermore, Fig. 3(c) shows the increased absorption at the quarter-wave condition owing to the destructive interference of the low-frequency sound waves, likely due to the air gap effect, as reported in literature [23,31].

Fig. 4 shows the sound absorption coefficient results which were determined for the various multilayered structures. As demonstrated in Fig. 1 in the SEM images, sample A contains the largest cavities and pores, while the open porosity is the highest in sample B. This specific characteristic of the sample morphology is strongly related to the resulting sound absorption coefficient of the multilayered foams. Fig. 4(a) shows the sound absorption coefficients of the double-layered specimens, revealing almost perfect sound absorption for frequencies higher than 2,000 Hz for sample BD. The double-layered specimens (solid lines) with the B layer in front generated higher sound absorption coefficients than those with the A layer in the front (dashed-dotted lines). This could be attributed to the combination of the highly open porosity of the B

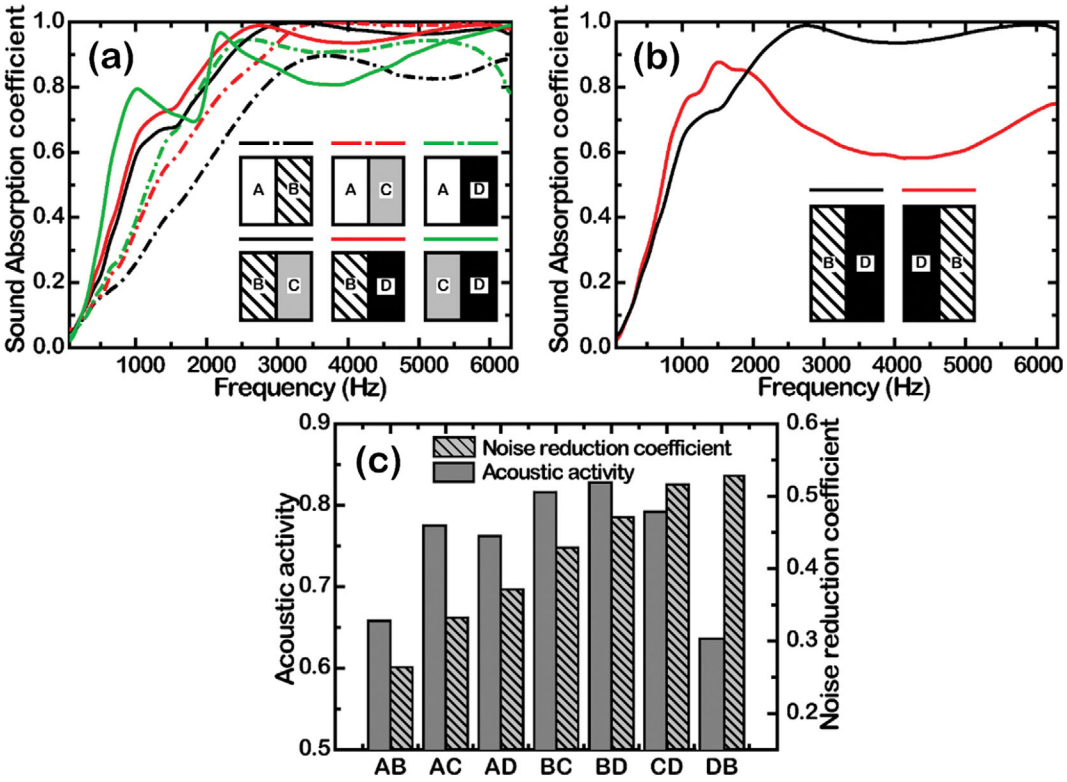

Fig. 4. (a) Sound absorption coefficients of the various double-layered specimens; (b) comparison between the sound absorption coefficients of samples BD and DB to establish the combination sequence effect on the sound absorption; (c) acoustic activity and noise reduction coefficient results for all the double-layered PUF specimens.

layer, which dissipates high-frequency waves, and the small cavities of the C or D layer, which diffracts low-frequency waves. In addition, the CD sample produced a high sound absorption coefficient for the low frequency specified waves because of the small cavity sizes in both layers. Fig. 4(b) demonstrates the importance of combination sequences on the sound absorption coefficients in double-layered materials. As shown in Fig. 4(a), sample BD exhibits the highest sound absorption coefficient, but its reverse order produces a significantly different result. Owing to a reduction in the passages of the high-frequency waves through the front layer (D), the sound absorption coefficient decreases significantly at frequency higher than 2,000 Hz. However, it is slightly enhanced in the low-frequency range because of the destructive interference effect of the low-frequency waves through the back layer (B), as shown schematically in Fig. 3(c).

Finally, Fig. 4(c) shows the AA and NRC of all the double layered PUF specimens. Overall, the BD sample combination exhibits the highest AA, and sample DB shows the highest NRC value. The NRC is strongly related to the sound absorption at frequencies lower than 2,000 Hz; thus, sample DB has a higher NRC than sample BD (see Fig. 4(b)). As a result, the double-layered BD sample showed the best sound absorption performance because the AA was significantly improved from 0.76 (monolayer B) to 0.82. Therefore, sequential arrangements of cellular morphology can be used to enhance the sound absorption performance of PUFs.

CONCLUSIONS

Four different PUF cellular morphologies were fabricated by utilizing low molecular weight polyols and two types of gelling catalysts. The cavity and pore sizes of the samples ranged from 458 μm and 143 μm to 287 μm and 86 μm, respectively. The open porosity and cell wall area ratio of the samples ranged from 0.97 and 0.59 to 0.63 and 0.80, respectively. The highest AA achieved for the monolayer PUF was 0.76. However, this was increased to 0.82 in the double-layered BD sample due to the synergistic effects between the front B layer, which exhibits highly open porosity for dissipating high-frequency waves, and the back D layer, which contains small cavities for diffracting low-frequency waves. By utilizing layer combinations with various cellular structures, the sound absorption performance can be further modulated in PUF systems. This design concept can also be applied to a variety of practical engineering problems.

ACKNOWLEDGEMENTS

This work was supported by the Basic Science Research Program through the National Research Foundation of Korea (NRF) funded by the Ministry of Science and ICT (NRF-2018R1D1A1 A09082239).

REFERENCES

1. H. Choe, Y. Choi and J. H. Kim, *J. Ind. Eng. Chem.*, **73**, 344 (2019).
2. G. Sung, J. W. Kim and J. H. Kim, *J. Ind. Eng. Chem.*, **44**, 99 (2016).
3. A. Kausar, *Polym. Plast. Technol. Eng.*, **57**, 346 (2018).
4. C. Zhang, J. Li, Z. Hu, F. Zhu and Y. Huang, *Mater. Des.*, **41**, 319 (2012).
5. J. G. Gwon, S. K. Kim and J. H. Kim, *Mater. Des.*, **387**, 448 (2015).
6. W. J. Yang, G. Y. Lee and S. H. Park, *Int. J. Precis. Eng. Manuf.*, **20**, 2041 (2019).
7. H. J. Choi and J. H. Kim, *Polym. Korea*, **45**, 143 (2021).
8. J. Hyuk, S. Hyun, H. Rae, C. Bin, S. Yeol, C. Sung, Y. June and J. Ryoun, *J. Sound Vib.*, **397**, 17 (2017).
9. L. Cao, Q. Fu, Y. Si, B. Ding and J. Yu, *Compos. Commun.*, **10**, 25 (2018).
10. C. H. Sung, K. S. Lee, K. S. Lee, S. M. Oh, J. H. Kim, M. S. Kim and H. M. Jeong, *Macromol. Res.*, **15**, 181 (2008).
11. G. Sung and J. H. Kim, *Compos. Sci. Technol.*, **146**, 147 (2017).
12. H. Choe, G. Sung and J. H. Kim, *Compos. Sci. Technol.*, **156**, 19 (2018).
13. S. H. Baek and J. H. Kim, *Compos. Sci. Technol.*, **198**, 108325 (2020).
14. J. H. Oh, J. S. Kim, V. H. Nguyen and I. K. Oh, *Compos. Part B Eng.*, **186**, 107817 (2020).
15. M. J. Nine, M. Ayub, A. C. Zander, D. N. H. Tran, B. S. Cazzolato and D. Losic, *Adv. Funct. Mater.*, **27**, 1 (2017).
16. S. H. Baek, H. J. Choi and J. H. Kim, *Polym. Korea*, **44**, 91 (2020).
17. S. K. Kim, G. Sung, J. G. Gwon and J. H. Kim, *Int. J. Precis. Eng. Manuf. - Green Technol.*, **3**, 367 (2016).
18. H. Choe and J. H. Kim, *J. Ind. Eng. Chem.*, **69**, 153 (2019).
19. Y. Wang, C. Zhang, L. Ren, M. Ichchou, M. A. Galland and O. Bareille, *Polym. Compos.*, **34**, 1847 (2013).
20. S. Chen and Y. Jiang, *Polym. Compos.*, **39**, 1370 (2018).
21. J. H. Oh, J. Kim, H. Lee, Y. Kang and I. K. Oh, *ACS Appl. Mater. Interfaces*, **10**, 22650 (2018).
22. G. Sung, H. Choe, Y. Choi and J. H. Kim, *Korean J. Chem. Eng.*, **35**, 1045 (2018).
23. N. Jingfeng and Z. GuiPing, *JVC/Journal Vib. Control*, **22**, 2861 (2016).
24. P. Bai, X. Yang, X. Shen, X. Zhang, Z. Li, Q. Yin, G. Jiang and F. Yang, *Mater. Des.*, **167**, 107637 (2019).
25. X. Shen, P. Bai, X. Yang, X. Zhang and S. To, *Appl. Sci.*, **9**, 1507 (2019).
26. J. G. Gwon, G. Sung and J. H. Kim, *Int. J. Precis. Eng. Manuf.*, **16**, 2299 (2015).
27. H. J. Choi and J. H. Kim, *J. Ind. Eng. Chem.*, **90**, 260 (2020).
28. H. J. Choi, H. Choe, W. J. Seo and J. H. Kim, *Polym. Korea*, **43**, 532 (2019).
29. R. Verdejo, R. Stämpfli, M. Alvarez-Lainez, S. Mourad, M. A. Rodriguez-Perez, P. A. Brühwiler and M. Shaffer, *Compos. Sci. Technol.*, **69**, 1564 (2009).
30. G. Sung, J. S. Kim and J. H. Kim, *Polym. Adv. Technol.*, **29**, 852 (2018).
31. M. B. Mvubu, R. Anandjiwala and A. Patnaik, *J. Eng. Fiber. Fabr.*, **14**, 874 (2019).